Accepted Manuscript

Synthesis of Co_3O_4–ZnO mixed metal oxide nanoparticles by homogeneous precipitation method

Ravi Kant Sharma, Ranjana Ghose

PII: S0925-8388(16)31659-0

DOI: 10.1016/j.jallcom.2016.05.298

Reference: JALCOM 37818

To appear in: *Journal of Alloys and Compounds*

Received Date: 24 February 2016

Revised Date: 24 May 2016

Accepted Date: 27 May 2016

Please cite this article as: R.K. Sharma, R. Ghose, Synthesis of Co_3O_4–ZnO mixed metal oxide nanoparticles by homogeneous precipitation method, *Journal of Alloys and Compounds* (2016), doi: 10.1016/j.jallcom.2016.05.298.

Synthesis of Co_3O_4–ZnO mixed metal oxide nanoparticles by homogeneous precipitation method

*Ravi Kant Sharma and Ranjana Ghose**

Department of Chemistry

Indian Institute of Technology (B.H.U)

Varanasi-221005, India

Abstract

Co_3O_4–ZnO mixed metal oxide nanoparticles have been successfully prepared by a simple and surfactant-free homogeneous precipitation method in short time followed by calcination at low temperature (350 ^oC). The synthesized samples were characterized by means of a multitechnique approach involving powder X-ray diffraction, thermal gravimetric analysis, Fourier transform infrared spectroscopy, UV-Visible diffuse reflectance spectroscopy, X-ray photoelectron spectroscopy, surface area measurements, scanning electron microscopy coupled with energy dispersive X-ray analysis, transmission electron microscopy and a superconducting quantum interference device magnetometer. From the magnetic measurements Co_3O_4–ZnO mixed metal oxide nanoparticles were found to be weak ferromagnetic behavior at low temperature (10 K).

Keywords: X-ray methods; Magnetic properties; Mixed metal oxide nanoparticles; Homogeneous precipitation method; Optical properties.

*Corresponding author:

Tel. +910542-6702879; Fax. +915422368428; E-mail: rghose.iitbhu.ac.in@gmail.com

1. Introduction

By upcoming of nano-materials a remarkable effort has been made for investigating on their significant properties which improve their use in many scientific fields. Co_3O_4 nanoparticles are of great importance due to their interesting electronic, electrical, optical, photochemical and magnetic properties [1-4]. They are extensively used in numerous areas such as catalysts, adsorbents, gas sensors, electrochromic devices, lithium ion batteries, supercapacitors, energy storage devices, solar-selective absorbers, drug delivery, biodiagnostics and magnetic recording media [2, 5-9]. Co_3O_4 is a magnetic p-type semiconductor with a direct optical band gaps of 1.48 and 2.19 eV [10], while ZnO is an n-type semiconductor with a wide direct band-gap (3.3–3.6 eV) and has high exciton binding energy of 60 mV at room temperature [11]. Due to this ZnO nanoparticles are being used in transparent conductive coatings, light-emitting diodes, hydrogen storage devices, varistor and UV lasers [12-15]. The superior functional performances like photocatalytic, optoelectronic and gas sensing of Co_3O_4–ZnO mixed metal oxide nanoparticles in comparison to the corresponding single-phase semiconductor oxides are mostly attributed to the build-up of an inner electric field at the p/n junction interface and enhanced separation of electron/hole carriers [16-19]. The diode fabricated using p-type Co_3O_4 nanoplate/n-type ZnO nanorods showed reasonable electrical performance [20]. The catalytic behavior was observed by the synthesized Co_3O_4/ZnO systems in the production of glycerol carbonate [21], catalytic oxidation of CO by O_2 [22] and low-temperature N_2O decomposition reaction [23]. The Co_3O_4/ZnO core/shell nanorods exhibit enhancement of photocatalytic activity in degradation of methylene blue than single Co_3O_4 nanorods component [24]. They are also indicating attractive performances in the detection of flammable/toxic analytes (CH_3CH_2OH, CH_3COCH_3, NO_2) [16, 18]. Hu et al. have reported high power Co_3O_4/ZnO p–n type piezoelectric transducer which can be operated at low frequencies [25]. Kandjani et al. have

explored the optical and magnetic properties of Co_3O_4–ZnO nanoparticles [26]. According to the earlier research, the physicochemical properties of the Co_3O_4-based materials are generally affected by their morphologies, structures, chemical composition and sizes [27, 28]. For the synthesis of mixed metal oxide nanoparticles, various methods such as, electrochemical [29], inverse microemulsion [30], hydrothermal [31], solvothermal [32], thermal decomposition [33], electrospinning [34], microwave-assisted [35], high energy mechanical ball milling [36], thermal evaporation [37] and sol-gel [38] processes have been employed. However, most of these approaches generally require high reaction temperature, tedious procedures, high-energy, long reaction time, expensive equipments, and harmful organic reagents or surfactants, which might further hinder their application. Among many methods developed for the synthesis of mixed metal oxide nanoparticles the homogeneous precipitation method is the most convenient and useful technique because it not only enables to avoid complicated processes, special instruments and severe preparation conditions but also provides easy control of particle size and shape [39, 40].

The plasma enhanced-chemical vapor deposition process used by Bekermann et al. [41] needs Ar and O_2 as plasma sources for the synthesis of Co_3O_4–ZnO nanoparticles. Dong et al. [24] prepared the nanoparticles by hydrothermal method using dimethylformamide (DMF) with longer reaction time (12 h) while Jana et al. [42] have employed the surfactant triethanolamine (TEA) for its preparation by a chemical route. Kanjwal et al. [43] required poly vinyl alcohol (PVA), a high-voltage power supply (source of the electric field) and longer time (24 h) in an electrospinning process followed by a hydrothermal technique. Zhang et al. [44] have used polyvinyl pyrrolidone (PVP), ethylene glycol (EG) and teflon-lined stainless steel autoclave in a solvothermal method. In the present work Co_3O_4–ZnO mixed metal oxide nanoparticles with high purity has been synthesized by homogeneous precipitation method which is a simple, inexpensive, environmentally friendly without using

any organic additive or surfactant and samples were prepared at low temperature in short time in large scale production. After thorough characterization, optical and magnetic properties of the nanoparticles were also investigated.

2. Experimental

2.1. *Materials*

The chemicals used were cobalt (II) oxalate dihydrate ($CoC_2O_4 \cdot 2H_2O$) (SIGMA ALDRICH®), zinc (II) acetate dihydrate ($Zn(CH_3COO)_2 \cdot 2H_2O$) (MERCK®) and ammonia solution (25%, RANKEM®). All the chemicals were analytical grade and were used as reagents as received without further purification. The solutions were prepared in Millipore® water.

2.2. Synthesis

In the present study, Co_3O_4–ZnO mixed metal oxide nanoparticles were prepared through proper precursors by a surfactant-free homogeneous precipitation method. The synthetic details are as follows.

In a 250 mL beaker 90 mL aqueous solution of cobalt oxalate (8 mmol) and 90 mL aqueous solution of zinc acetate (8 mmol) were taken. Subsequently, 14 mL of 25% aqueous ammonia solution (ammonium hydroxide) was added dropwise into the above mixture and the contents were heated to ~ 80 ^oC with continuous stirring for 2 h. During the reaction a light pink precipitate formed which was filtered off, washed first with water four times to remove any impurity, then with ethyl alcohol two times and dried in an oven at 75 ^oC. The as prepared sample was grounded to fine powder with the help of a mortar and pestle. Finally calcination of the as-prepared powder was carried out in air at 350 ^oC and 500 ^oC at a heating rate of 2 ^oC/min for 3 h inside a muffle furnace. The colors of the samples before and after calcination were light pink and black respectively.

2.3. Characterization

Structural characterization of the as-prepared and calcined Co_3O_4–ZnO mixed metal oxide nanoparticles were performed using powder X-ray diffraction (XRD) patterns recording on a Bruker AXS-D8 diffractometer for 2θ values ranging from 10 to 80^o operating with Cu-Kα radiation (λ = 0.15406 nm) with a scanning speed of 2^o/min. Perkin Elmer Pyris Diamond instrument was used for thermogravimetric analysis (TGA) of the as-prepared sample in air in the temperature range from 25 to 800 ^{o}C with a heating rate of 5 ^{o}C/min. Diffuse reflectance spectra were recorded with the help of Shimadzu UV-2450 UV-Visible spectrophotometer attached with a diffuse reflectance accessory in the wavelength range 200 to 800 nm employing $BaSO_4$ as the reference. FT-IR spectra were taken with a NEXUS Thermo Nicolet IR-spectrometer in the range 4000-400 cm^{-1} with a spectral resolution of 2 cm^{-1} using KBr disk method for determining the functional groups. X-ray photoemission spectroscopy (XPS) spectra of the samples were executed on a KRATOS (Amicus model) high-performance analytical instrument using Mg target under 1.0×10^{-6} Pa pressure. Surface areas of the samples were measured with a Micromeritics Chemisorb 2720 instrument by Brunauer-Emmett-Teller (BET) method using nitrogen physisorption at 77 K. The morphology of the samples was investigated using a scanning electron microscope (SEM: EVO 18, Carl Zeiss microscopy Ltd.) operating at an accelerating voltage of 20 kV coupled with an energy dispersive X-ray analysis (EDXA) facility. TEM images of the Co_3O_4–ZnO mixed metal oxide nanoparticles were obtained using a FEI TECNAI G2 transmission electron microscope functioning at an accelerating voltage of 200 kV. For TEM measurements the powder samples were dispersed in ethanol with a low power sonication. A few drops of ethanol suspensions of the powders were dispersed onto carbon coated copper grids which was allowed to dry at room temperature. Magnetic measurements were done on a superconducting quantum interference device (SQUID) (Quantum Design,

MPMS 3). Field-dependent magnetization curves were obtained at 10 and 300 K up to a maximum field of 7 T. Temperature-dependent magnetization curves were recorded under zero field cooled (ZFC) and field cooled (FC) conditions from 2 to 300 K under an applied field of 500 Oe.

3. Results and discussion

Appropriate amount of ammonium hydroxide was added to a mixture of aqueous cobalt oxalate and aqueous zinc acetate solution with continuous stirring for 2 h at about 80 ^{o}C and the following reactions take place:

$$6CoC_2O_4 \cdot 2H_2O\ (aq.) + 6Zn(CH_3COO)_2 \cdot 2H_2O\ (aq.) + 24NH_4OH\ (aq.) \xrightarrow{80\ ^{o}C,\ 2h}$$

$$3Zn(OH)_2 + 3Zn(CH_3COO)_2(NH_3)_2 + 3Co(OH)_2 + Co_3O_4 + 6(NH_4)_2C_2O_4 + 6CH_3COONH_4 + 32H_2O + H_2\ (g) \quad (1)$$

After calcination

$$Zn(CH_3COO)_2(NH_3)_2 + [O] \longrightarrow ZnO + C_2H_6\ (g) + 2CO_2\ (g) + 2NH_3\ (g) \quad (2)$$

$$Zn(OH)_2 \longrightarrow ZnO + H_2O \quad (3)$$

$$3Co(OH)_2 \longrightarrow Co_3O_4 + 2H_2O + H_2\ (g) \quad (4)$$

After calcination the formation of pure Co_3O_4–ZnO mixed metal oxide nanoparticles is evidenced by the XRD data.

The X-ray powder diffraction results of the as-prepared and calcined (350 ^{o}C and 500 ^{o}C) samples are shown in Fig. 1. XRD pattern of the as-prepared sample shows four phases: one due to β-$Zn(OH)_2$ (JCPDS file no. 20-1435), second due to zinc acetate ammonia ($Zn(CH_3COO)_2(NH_3)_2$) (JCPDS file no. 21-1468), third due to β-$Co(OH)_2$ (JCPDS file no. 51-1731) and the fourth due to Co_3O_4. After calcination at 350 ^{o}C and 500 ^{o}C diffraction peaks were observed at $2\theta \approx 18.97^{o}$, 31.32^{o}, 36.87^{o}, 38.58^{o}, 44.89^{o}, 55.64^{o}, 59.40^{o} and 65.25^{o} which are indexed at diffraction lines of (111), (220), (311), (222), (400), (422), (511) and

(440) respectively corresponding to typical cubic spinel structure Co_3O_4 which is in good agreement with JCPDS No. 42–1467. In the same XRD pattern diffraction peaks of hexagonal ZnO with lattice parameters of a = 0.3250 nm and c = 0.5207 nm were also obtained at $2\theta \approx 34.36^o$, 56.58^o, 62.87^o, 67.91^o, 69.0^o, 72.68^o and 76.89^o which are indexed to the (002), (110), (103), (112), (201), (004) and (202) diffraction lines respectively (JCPDS file no. 79-2205). The XRD patterns confirm the formation of pure Co_3O_4–ZnO mixed metal oxide after calcination. The crystallite sizes of the calcined samples were calculated by means of the Debye-Scherrer equation as given below [45].

$$\delta = 0.89\,\lambda/\,\beta\cos\theta \qquad (5)$$

where δ is the crystallite size in nanometers, 0.89 represents a dimensionless constant k, λ is the wavelength of Cu-Kα (0.15406 nm), β is the full width at half maximum (FWHM, radian) of the chosen diffraction peak (corrected for experimental broadening) and θ is the diffraction angle (degree). The crystallite size of Co_3O_4 is 8.3 nm in the sample calcined at 350 ^oC while it is 12.7 nm in the sample calcined at 500 ^oC. It is found from the XRD analyses that on increasing calcination temperature the intensity of the diffraction peaks also increase which is ascribed to the larger crystallite size.

The thermal gravimetric analysis pattern for as-prepared powder is shown in Fig. 2. The overall weight losses (about 39.4 %) between 25-350 ^oC are attributed to the dehydration of metal hydroxide to metal oxide and also to the removal of inorganic and organic matters obtained from the decomposition of zinc acetate ammonia [48, 50]. There is no weight loss after 350 ^oC confirming the formation of Co_3O_4–ZnO mixed metal oxide.

The FT-IR spectra of as-prepared and calcined (350 ^oC and 500 ^oC) samples are presented in Fig. 3. The broad band at around 3545–3357 cm^{-1} in the spectra of as-prepared sample is ascribed to the stretching vibrations of –OH and –NH which does not appear in the calcined sample [46]. The band at about 2930 cm^{-1} is attributed to C–H stretching in the spectra of the

as-prepared sample [47]. In the spectrum of the as-prepared sample the bands at 1330 and 1625 cm^{-1} are assigned to the binding of acetate ion to zinc (II) and these disappear in case of calcined samples [48]. The band at 1249 cm^{-1} is due to –C–O stretching in the spectra of as-prepared sample [49]. The bands at 490 and 777 cm^{-1} are associated with Co-O stretching and Co-OH bending vibrations in the spectra of the as-prepared sample [50]. The bands appearing at about 565 (ν_1) and 664 (ν_2) cm^{-1} originate from the stretching vibrations of the Co–O bonds in the spectra of calcined samples [51]. The ν_1 band is due to Co^{3+}–O vibration in the octahedral hole and ν_2 band is a characteristic of Co^{2+}–O vibration in tetrahedral hole in the spinel lattice [52]. The lower frequency band at 468 cm^{-1} is attributed to the Zn-O stretching vibrations in the spectra of the calcined samples [53].

X-ray photoelectron spectroscopy (XPS) is a quantitative spectroscopic method that determines the chemical-states of the elements present in the materials. The XPS spectra of Co 2p, Zn 2p, and O 1s in Co_3O_4–ZnO mixed metal oxide nanoparticles are shown in Fig. 4(a). The peaks of Co $2p_{3/2}$ and Co $2p_{1/2}$ correspond to the binding energy of 780.3 eV and 795.7 eV respectively (Fig. 4(b)) which matches with the binding energy of Co_3O_4 of the earlier work [54]. In Fig. 4(c), the binding energy for spin orbit doublet peaks of the Zn $2p_{3/2}$ and Zn $2p_{1/2}$ in ZnO appeared at about 1021.7 eV and 1045.2 eV respectively which are consistent with other reports [55]. Two peaks are clearly marked at 529.9 eV and 531.3 eV for O 1s spectrum of the Co_3O_4–ZnO mixed metal oxide nanoparticles (Fig. 4(d)). The main low-energy oxygen peak at 529.9 eV is assigned to the lattice oxygen (O^{2-}) present in the Co_3O_4–ZnO mixed metal oxide nanoparticles [24]. The second peak at higher binding energy (531.3 eV) is similar to that reported for the surface hydroxyls and chemisorbed oxygen [24, 56]. The XPS analysis of the samples gives the atomic ratio of Co to Zn as 2.87 (at. % Co = 31.24 and Zn = 10.87) and 2.94 (at. % Co = 33.11 and Zn = 11.26) in the calcined samples at 350 ^oC and 500 ^oC respectively. XPS compositional analyses supported the presence of

Co_3O_4 and ZnO in the mixed metal oxide nanoparticles. The XPS results are in good agreement with XRD measurements.

UV–visible diffuse reflectance spectroscopy is one of the most important techniques to reveal the band structure or molecular energy levels in the semiconductor materials. Diffuse reflectance spectra of the calcined samples at 350 ^oC and 500 ^oC are presented in Figs. 5(a) and (b). The UV-visible spectra of the samples calcined at 350 ^oC and 500 ^oC exhibit one band at 363 nm and 374 nm, respectively. Kubelka–Munk formula [15] is used to calculate the optical absorption coefficient (α):

$$\alpha = (1-R)^2/2R \qquad (6)$$

where R is the diffuse reflectance. The optical band gap (E_g) of Co_3O_4–ZnO mixed metal oxide nanoparticles is determined by extrapolation of the linear relationship between $(\alpha h\upsilon)^2$ and $(h\upsilon)$ [8] :

$$(\alpha h\upsilon)^2 = K(h\upsilon - E_g) \qquad (5)$$

where K is proportionality constant and υ is the frequency of photons. The $(\alpha h\upsilon)^2$ on the y axis versus photo energy $(h\upsilon)$ on the x-axis are plotted in Figs. 5(c) and (d) on the basis of data obtained from Figs. 5(a) and (b). The estimated band-gap energy, thus obtained, are ~ 3.41 and 3.31 eV for samples calcined at 350 ^oC and 500 ^oC respectively [26]. Generally the optical band gap is influenced by several factors such as morphology, compositions, surface defect states (oxygen vacancies) and quantum confinement effects of the nanoparticles [40, 58]. The optical properties of Co_3O_4–ZnO mixed metal oxide nanoparticles are important for solar cells, electrochromic devices and gas sensor applications.

The specific surface area of as-prepared and calcined Co_3O_4–ZnO samples was measured using BET (Brunauer–Emmett–Teller) method and the results are given in Table 1. The BET results indicate that Co_3O_4–ZnO mixed metal oxide calcined at 350 ^oC has high specific surface area (72.4 m^2g^{-1}) in comparison to the as-prepared (SSA ~ 16.7 m^2g^{-1}) and calcined

sample at 500 ^{o}C (SSA ~ 67.8 m^2g^{-1}). The specific surface area of Co_3O_4–ZnO mixed metal oxide nanoparticles synthesized by other techniques like the hydrothermal [26], solvothermal [44] and thermal decomposition [59] are significantly lower (54.6 m^2g^{-1}, 60.9 m^2g^{-1} and 46.9 m^2g^{-1} respectively) than those obtained in the present method.

SEM images of the as-prepared and calcined samples at 350 ^{o}C and 500 ^{o}C show agglomeration of nanoparticles (Figs. 6(a)-(c)). The growth mechanism of the nanoparticles explained on the basis of precipitation, dissolution, renucleation, growth, aggregation [60, 61]. First on supersaturation the primary precipitates were formed. This was followed by dissolution of unstable precipitates which on renucleation and growth of crystallites takes place. The resultant crystallites were aggregated or attached onto the final crystals to minimize the interfacial energy.

The EDX analyses results indicate the presence of cobalt, zinc and oxygen elements in the as-prepared and calcined samples (Fig. 6(d)). The EDX analysis data of the samples give the atomic ratio of Co to Zn as 2.98 and 3.00 in the calcined samples at 350 ^{o}C and 500 ^{o}C respectively (Table 2) which is closely match with the XPS results. The EDX analyses data show almost uniform distribution of cobalt, zinc and oxygen elements throughout the whole mixed metal oxide nanoparticles structure.

TEM images of the Co_3O_4–ZnO mixed metal oxide nanoparticles after calcination at 350 ^{o}C showed in Figs. 7(a) and (b). It is seen that the darker parts of the image is similar to a spherical shape, they are related to Co_3O_4 whereas brighter irregular-shapes are related to ZnO in sample. The corresponding selected-area electron diffraction (SAED) pattern (Fig. 7(c)) of the mixed metal oxide nanoparticles showed several distinct concentric rings suggesting that the sample is polycrystalline in nature. The estimated average particle size of Co_3O_4 in mixed metal oxide nanoparticles is in the range 9.5–11.3 nm which is in agreement

with the value calculated from XRD measurements. A pictorial model showing the mixed metal oxide nanoparticles is demonstrated in Fig 7(d).

Variation in magnetization versus magnetic field measurements *(M–H*) at 300 K and 10 K for Co_3O_4–ZnO mixed metal oxide nanoparticles are shown in Fig. 8. At 300 K *M* varies linearly with *H* up to 60 kOe implying the magnetic interaction is of paramagnetic (PM) behaviour in the mixed metal oxide sample. In this case the magnetization is not saturated even at an applied field of 70 kOe suggesting progressive spin alignment along the external field. While the *M–H* curve for the sample at 10 K gives the fine shape to the hysteresis loop which is a characteristic of weak ferromagnetic nature. From the inset of Fig. 8 the estimated remanent magnetization (*Mr*) and coercive field (*Hc*) are 0.0068 emu/g and 175 Oe respectively. The low coercive field and remanent magnetization confirm weak ferromagnetic properties for the mixed metal oxide nanoparticles. It also justifies spontaneous spin alignment by the external magnetic field in the mixed metal oxide sample at low temperature. The hysteresis loop at 10 K gets broadened and is shifted towards negative field (see the inset in Fig. 8) with a small exchange anisotropy of H_{ex} = –36.5 Oe. It is attributed to the presence of uncompensated spin at the interface of the sample in the frozen state [62]. Exchange bias is the shift of the hysteresis loop along the direction of magnetic field axis. It arises from the coupling at the interface between Co_3O_4 antiferromagnetic core and uncompensated ferromagnetic moments at the surface [42]. Exchange bias depends on different parameters such as spin orientation or anisotropy, roughness, spin configuration, magnetic domains and atomic intermixing at the interface [63]. According to the reported mechanism [64] the exchange bias effect is schematically shown in Fig. 9. In the range $T_N < T < T_C$, the cooling field induces the alignment of the ferromagnetic (FM) spins along its direction (Fig. 9(i)) while at $T < T_N$ the spins of the antiferromagnetic (AFM) phase arrange in an antiferromagnetic configuration (Fig. 9(ii)). When the magnetic field is reversed, the FM spins have a tendency to reorient

while the AFM spins remain unchanged due to the large AFM anisotropy (Figs. 9(iii)-(v)). The ferromagnetic interaction at the FM-AFM interface gives a strong restoring force on the FM spins reorientations and therefore a shift of the M-H loop is produced. The temperature dependence of zero-field-cooled (ZFC) and field-cooled (FC) magnetization curves for the Co_3O_4–ZnO mixed metal oxide nanoparticles under an applied field of 500 Oe are presented in Fig. 10. It is already known that bare ZnO has no magnetic character, while bulk Co_3O_4 is an antiferromagnetic with the Neel temperature T_N = 40 K [65]. For bulk antiferromagnetic materials the net magnetization is zero due to complete compensation of sublattice magnetizations. Co_3O_4–ZnO mixed metal oxide nanoparticles show the blocking temperature (T_B) at about 38 K in the curves (Fig. 10) which corresponds to the magnetic transition in the mixed metal oxide nanoparticles. In the *M–T* characteristic curves of the sample M_{ZFC} and M_{FC} lines get separated below 38 K temperature. The most interesting observation for the Co_3O_4–ZnO mixed metal oxide nanoparticles is that on decreasing temperature both M_{ZFC} and M_{FC} data start to increase nearly at 38 K. The increment in the magnetic moment of the material at this low temperature is attributed to the interface effect of the mixed metal oxide nanoparticles [42]. At the low thermal energy (< 38 K) uncompensated surface spins and/or finite size effects of the mixed metal oxide nanoparticles makes it behave similar to the ferromagnetic spins and they can spontaneously be aligned by the external magnetic field.

4. Conclusions

The synthesis of pure Co_3O_4–ZnO mixed metal oxide nanoparticles has been carried out via a simple homogeneous precipitation method in short time at low calcination temperature and in large scale production without using any surfactant/chelating agent. The synthesized samples have been characterized using an array of analytical techniques. The estimated optical band-gap value are 3.41 and 3.31 eV for Co_3O_4–ZnO mixed metal oxide nanoparticles calcined at 350 ^{o} and 500 ^{o}C respectively. The mixed metal oxide nanoparticles obtained in the present

work show high surface area. This method may be extended to the preparation of other mixed metal oxide nanoparticles. The prepared Co_3O_4–ZnO mixed metal oxide nanoparticles exhibit weak ferromagnetic behavior at low temperature with low coercive field (175 Oe) and remanent magnetization (0.0068 emu/g). The perspective applications of Co_3O_4–ZnO mixed metal oxide nanoparticles include sensing, photocatalysis and optoelectronics.

Acknowledgement

Ravi Kant Sharma would like to thank the Ministry of Human Resource and Development, Government of India, for providing financial support during the research work. We are thankful to Professor U.P Singh, Department of Chemistry, IIT, Roorkee for helping in carrying out the present work. Thanks are also to Central Instrument Facility, IIT (BHU) for providing the facilities.

References

[1] S.A. Makhlouf, Z.H. Bakr, K.I. Aly, M.S. Moustafa, Structural, electrical and optical properties of Co_3O_4 nanoparticles, Superlattices and Microstructures 64 (2013) 107–117.

[2] N.A.M. Barakat, M.S. Khil, F.A. Sheikh, H.Y. Kim, Synthesis and optical properties of two cobalt oxides (CoO and Co_3O_4) nanofibers produced by electrospinning process, Journal of Physical Chemistry C 112 (2008) 12225–12233.

[3] S.A. Makhlouf, Magnetic properties of Co_3O_4 nanoparticles, Journal of Magnetism and Magnetic Materials 246 (2002) 184–190.

[4] M. Grzelczak, J. Zhang, J. Pfrommer, J. Hartmann, M. Driess, M. Antonietti, X. Wang, Electro- and photochemical water oxidation on ligand-free Co_3O_4 nanoparticles with tunable sizes, ACS Catalysis 3 (2013) 383−388.

[5] Z. Dong, Y. Fu, Q. Han, Y. Xu, H. Zhang, Synthesis and physical properties of Co_3O_4 nanowires, Journal of Physical Chemistry C 111 (2007) 18475−18478.

[6] X.J. Ma, Y.J. Yu, J.L. Xing, T.Q. Yang, K.F. Lam, Q.S. Xue, B. Albela, L. Bonneviot, K. Zhang, Tailoring porosity and dimensionality of Co_3O_4 nanophase using channel interconnectivity control by steaming of nanocasting SBA-15, Microporous and Mesoporous Materials 200 (2014) 182–189.

[7] G.G. Pacheco, J.G.C. Moreno, H.Y. Madeira, F.C. Gandarilla, Co_3O_4 nanoparticles produced by mechanochemical reactions, Nanotechnology 17 (2006) 2528–2535.

[8] A. Matsuda, R. Yamauchi, D. Shiojiri, G. Tan, S. Kaneko, M. Yoshimoto, Room-temperature selective epitaxial growth of CoO (1 1 1) and Co_3O_4 (1 1 1) thin films with atomic steps by pulsed laser deposition, Applied Surface Science 349 (2015) 78–82.

[9] X. Wang, L. Yu, X.L. Wu, F. Yuan, Y.G. Guo, Y. Ma, J. Yao, Synthesis of single-crystalline Co_3O_4 octahedral cages with tunable surface aperture and their lithium storage properties, Journal of Physical Chemistry C 113 (2009) 15553–15558.

[10] V.H. Nguyen, J.J. Shim, Ionic liquid-assisted synthesis and electrochemical properties of ultrathin Co_3O_4 nanotube-intercalated graphene composites, Materials Letters 157 (2015) 290–294.

[11] E. Darezereshki, M. Alizadeh, F. Bakhtiari, M. Schaffie, M. Ranjbar, A novel thermal decomposition method for the synthesis of ZnO nanoparticles from low concentration $ZnSO_4$ solutions, Applied Clay Science 54 (2011) 107–111.

[12] F. Soofivand, M.S. Niasari, F. Mohandes, Novel precursor-assisted synthesis and characterization of zinc oxide nanoparticles/nanofibers, Materials Letters 98 (2013) 55–58.

[13] Z. Jia, L. Yue, Y. Zheng, Z. Xu, Rod-like zinc oxide constructed by nanoparticles: synthesis, characterization and optical properties, Materials Chemistry and Physics 107 (2008) 137–141.

[14] O.A. Yildirim, C. Durucan, Synthesis of zinc oxide nanoparticles elaborated by microemulsion method, Journal of Alloys and Compounds 506 (2010) 944–949.

[15] F. Yakuphanoglu, Electrical characterization and device characterization of ZnO microring shaped films by sol–gel method, Journal of Alloys and Compounds507 (2010) 184–189.

[16] D. Bekermann, A. Gasparotto, D. Barreca, C. Maccato, E. Comini, C. Sada, G. Sberveglieri, A. Devi, R. A. Fischer, Co_3O_4/ZnO nanocomposites: from plasma synthesis to gas sensing applications, Applied Materials and Interfaces 4 (2012) 928−934.

[17] Z. Zhang, C. Shao, X. Li, C. Wang, M. Zhang, Y. Liu, Electrospun nanofibers of p-type NiO/n-type ZnO heterojunctions with enhanced photocatalytic activity, Applied Materials and Interfaces 2 (2010) 2915–2923.

[18] C.W. Na, H.S. Woo, I.D. Kim, J.H. Lee, Selective detection of NO_2 and C_2H_5OH using a Co_3O_4-decorated ZnO nanowire network sensor, Chemical Communications 47 (2011) 5148–5150.

[19] L.J. Zhuge, X.M. Wu, Z.F. Wu, X.M. Yang, X.M. Chen, Q. Chen, Structure and deep ultraviolet emission of Co-doped ZnO films with Co_3O_4 nano-clusters, Materials Chemistry and Physics120 (2010) 480–483.

[20] T.I. Lee, S.H. Lee, Y.D. Kim, W.S. Jang, J.Y. Oh, Hong, K. Baik, C. Stampfl, A. Soon, J.M. Myoung, Playing with dimensions: rational design for heteroepitaxial p−n junctions, Nano Letters 12 (2012) 68−76.

[21] F.R. Marcos, V.C. Casilda, M.A. Banares, J.F. Fernandez, Novel hierarchical Co_3O_4/ZnO mixtures by dry nanodispersion and their catalytic application in the carbonylation of glycerol, Journal of Catalysis 275 (2010) 288–293.

[22] G.A.E. Shobaky, A.M. Ghozza, Effect of ZnO doping on surface and catalytic properties of NiO and Co_3O_4 solids, Materials Letters 58 (2004) 699–705.

[23] G. Grzybek, P. Stelmachowski, P. Indyka, M. Inger, M. Wilk, A. Kotarba, Z. Sojka, Cobalt–zinc spinel dispersed over cordierite monoliths for catalytic N_2O abatement from nitric acid plants, Catalysis Today 257 (2015) 93–97.

[24] C. Dong, X. Xiao, G. Chen, H. Guan, Y. Wang, Synthesis and photocatalytic degradation of methylene blue over p-n junction Co_3O_4/ZnO core/shell nanorods, Materials Chemistry and Physics 155 (2015) 1–8.

[25] Y.C. Hu, T.H. Lee, P.Z. Chang, P.C. Su, High power Co_3O_4/ZnO p–n type piezoelectric transducer, Thin Solid Films 584 (2015) 112–115.

[26] A.E. Kandjani, S.E.H. Amiri, M.R. Vaezi, S.K. Sadrnezhaad, Optical and magnetic properties of Co_3O_4/ZnO Core/Shell nanoparticles, Journal of Optoelectronics and Advanced Materials 12 (2010) 2057–2062.

[27] M. Li, C. Han, Y. Zhang, X. Bo, L. Guo, Facile synthesis of ultrafine Co_3O_4 nanocrystals embedded carbon matrices with specific skeletal structures as efficient non-enzymatic glucose sensors, Analytica Chimica Acta 861 (2015) 25–35.

[28] K. Zhou, J. Liu, P. Wen, Y. Hu, Z. Gui, Morphology-controlled synthesis of Co_3O_4 by one step template-free hydrothermal method, Materials Research Bulletin 67 (2015) 87–93.

[29] R. Galindo, E. Mazario, S. Gutierrez, M.P. Morales, P. Herrasti, Electrochemical synthesis of $NiFe_2O_4$ nanoparticles: Characterization and their catalytic applications, Journal of Alloys and Compounds 536S (2012) S241–S244.

[30] L.M. Gan, L.H. Zhang, H.S.O. Chan, C.H. Chew, B.H. Loo, A novel method for the synthesis of perovskite-type mixed metal oxides by the inverse microemulsion technique, Journal of Materials Science 31 (1996) 1071–1079.

[31] J.R. Kim, K.Y. Lee, M.J. Suh, S.K. Ihm, Ceria–zirconia mixed oxide prepared by continuous hydrothermal synthesis in supercritical water as catalyst support, Catalysis Today 185 (2012) 25–34.

[32] M. Pang, G. Long, S. Jiang, Y. Ji, W. Han, B. Wang, X. Liu, Y. Xi, D. Wang, F. Xu, Ethanol-assisted solvothermal synthesis of porous nanostructured cobalt oxides (CoO/Co_3O_4) for high-performance supercapacitors, Chemical Engineering Journal 280 (2015) 377–384.

[33] X. Zhao, F. Zhang, S. Xu, D.G. Evans, X. Duan, From layered double hydroxides to ZnO-based mixed metal oxides by thermal decomposition: transformation mechanism and uv-blocking properties of the product, Chemistry of Materials 22 (2010) 3933–3942.

[34] J. Moon, J.A. Park, S.J. Lee, S.C. Lim, T. Zyung, Structure and electrical properties of electrospun ZnO–NiO mixed oxide nanofibers, Current Applied Physics 9 (2009) S213–S216.

[35] L. Gu, L. Qian, Y. Lei, Y. Wang, J. Li, H. Yuan, D. Xiao, Microwave-assisted synthesis of nanosphere-like $NiCo_2O_4$ consisting of porous nanosheets and its application in electro-catalytic oxidation of methanol, Journal of Power Sources 261 (2014) 317–323.

[36] M. Kakazey, M. Vlasova, Y. Vorobiev, I. Leon, M.C. Gonzalez, E.A.C. Urbiola, Processes of microstructural evolution during high-energy mechanical treatment of ZnO and black NiO powder mixture, Physica B 453 (2014) 116–122.

[37] A. Chrissanthopoulos, S. Baskoutas, N. Bouropoulos, V. Dracopoulos, P. Poulopoulos, S.N. Yannopoulos, Synthesis and characterization of ZnO/NiO p–n heterojunctions: ZnO nanorods grown on NiO thin film by thermal evaporation, Photonics and Nanostructures–Fundamentals and Applications 9 (2011) 132–139.

[38] E. Amini, M. Rezaei, Preparation of mesoporous Fe-Cu mixed metal oxide nanopowder as active and stable catalyst for low-temperature CO oxidation, Chinese Journal of Catalysis 36 (2015) 1711–1718.

[39] M. Zhang, G. Sheng, J. Fu, T. An, X. Wang, X. Hu, Novel preparation of nanosized ZnO–SnO_2 with high photocatalytic activity by homogeneous co-precipitation method, Materials Letters 59 (2005) 3641–3644.

[40] R.K. Sharma, R. Ghose, Synthesis of nanocrystalline CuO–ZnO mixed metal oxide powder by a homogeneous precipitation method, Ceramics International 40 (2014) 10919–10926.

[41] D. Bekermann, A. Gasparotto, D. Barreca, C. Maccato, M. Rossi, R. Matassa, I. Cianchetta, S. Orlanducci, M. Kete, U.L. Stangar, Epitaxial-like Growth of Co_3O_4/ZnO Quasi-1D Nanocomposites, Crystal Growth and Design 12 (2012) 5118−5124.

[42] T.K. Jana, A. Pal, K. Chatterjee, Magnetic and photocatalytic study of Co_3O_4–ZnO nanocomposite, Journal of Alloys and Compounds 653 (2015) 338−344.

[43] M.A. Kanjwal, F.A. Sheikh, N.A.M. Barakat, I.S. Chronakis, H.Y. Kim, Co_3O_4–ZnO hierarchical nanostructures by electrospinning and hydrothermal methods, Applied Surface Science 257 (2011) 7975–7981.

[44] L. Zhang, X. Jing, J. Liu, J. Wang, Y. Sun, Facile synthesis of mesoporous ZnO/Co_3O_4 microspheres with enhanced gas-sensing for ethanol, Sensors and Actuators B 221 (2015) 1492–1498.

[45] B.D. Cullity, S.R. Stock, Elements of X-ray Diffraction, Prentice Hall, Upper Saddle River, New Jersey, 2001.

[46] K. Cheng, D. Cao, F. Yang, Y. Xu, G. Sun, K. Ye, J. Yin, G. Wang, Facile synthesis of morphology-controlled Co_3O_4 nanostructures through solvothermal method with enhanced catalytic activity for H_2O_2 electroreduction, Journal of Power Sources 253 (2014) 214–223.

[47] R.K. Sharma, P. Jeevanandam, Thermal decomposition approach for the synthesis of silver–alumina nanocomposite powders, Ceramics International 39 (2013) 3337–3344.

[48] Y. Wang, Y. Li, Z. Zhou, X. Zu, Y. Deng, Evolution of the zinc compound nanostructures in zinc acetate single-source solution, Journal of Nanoparticle Research 13 (2011) 5193–5202.

[49] M.P. Contreras, R.Y. Avula, R.K. Singh, Evaluation of nano zinc (ZnO) for surface enhancement of ATR–FTIR spectra of butter and spread, Food and Bioprocess Technology 3 (2010) 629–635.

[50] S.W. Kim, B.J. Kwon, J.H. Park, M.G. Hur, S.D. Yang, H. Jung, γ-ray radiation induced synthesis and characterization of α-cobalt hydroxide nanoparticles, Bulletin of the Korean Chemical Society 31 (2010) 910–914.

[51] M.S. Niasari, A. Khansari, F. Davar, Synthesis and characterization of cobalt oxide nanoparticles by thermal treatment process, Inorganica Chimica Acta 362 (2009) 4937–4942.

[52] L. Wang, X. Liu, X. Wang, X. Yang, L. Lu, Preparation and electrochemical properties of mesoporous Co_3O_4 crater-like microspheres as supercapacitor electrode materials, Current Applied Physics 10 (2010) 1422–1426.

[53] P. Thangaraj, J. Rajan, S. Durai, S. Kumar, A.R. Phani, G. Neri, The role of albumen (egg white) in controlled particle size and electrical conductivity behavior of zinc oxide nanoparticles, Vacuum 86 (2011) 140–143.

[54] Y. Tak, K. Yong, A novel heterostructure of Co_3O_4/ZnO nanowire array fabricated by photochemical coating method, Journal of Physical Chemistry C 112 (2008) 74-79.

[55] O. Lupan, G.A. Emelchenko, V.V. Ursaki, G. Chai, A.N. Redkin, A.N. Gruzintsev, I.M. Tiginyanu, L. Chow, L.K. Ono, B.R. Cuenya, H. Heinrich, E.E. Yakimov, Synthesis and characterization of ZnO nanowires for nanosensor applications, Materials Research Bulletin 45 (2010) 1026–1032.

[56] E. McCafferty, J.P. Wightman, determination of the concentration of surface hydroxyl groups on metal oxide films by a quantitative XPS method, Surface and Interface Analysis 26 (1998) 549 –564.

[57] S. Farhadi, K. Pourzare, S. Sadeghinejad, Simple preparation of ferromagnetic Co_3O_4 nanoparticles by thermal dissociation of the $[Co^{II}(NH_3)_6](NO_3)_2$ complex at low temperature, Journal of Nanostructure in Chemistry 3 (2013) 1–7.

[58] A.K. Zak, M.E. Abrishami, W.H.A. Maji, R. Yousefi, S.M. Hosseini, Effects of annealing temperature on some structural and optical properties of ZnO nanoparticles prepared by a modified sol–gel combustion method, Ceramics International 37 (2011) 393–398.

[59] D. Zhu, F. Zheng, S. Xu, Y. Zhang, Q. Chen, MOF-derived self-assembled ZnO/Co_3O_4 nanocomposite clusters as high-performance anodes for lithium-ion batteries, Dalton Transactions 44 (2015) 16946–16952.

[60] M.A. Garakani, S. Abouali, B. Zhang, Z.L. Xu, J. Huang, J.Q. Huang, E.K. Heidari, J.K. Kim, Controlled synthesis of cobalt carbonate/graphene composites with excellent

supercapacitive performance and pseudocapacitive characteristics, Journal of Materials Chemistry A 3 (2015) 17827–17836.

[61] N.T.K. Thanh, N. Maclean, S. Mahiddine, Mechanisms of nucleation and growth of nanoparticles in solution, Chemical Reviews 114 (2014) 7610−7630.

[62] R.K. Sharma, D. Kumar, R. Ghose, Synthesis of nanocrystalline ZnO–NiO mixed metal oxide powder by homogeneous precipitation method, Ceramics International 42 (2016) 4090–4098.

[63] J. Nogues, I.K. Schuller, Exchange bias, Journal of Magnetism and Magnetic Materials 192 (1999) 203−232.

[64] J. Nogues, D. Lederman, T.J. Moran, I.K. Schuller, Positive exchange bias in FeF_2-Fe bilayers, Physical Review Letters 76 (1996) 4624−4627.

[65] S. Sharma, N. Garg, K.V. Ramanujachary, S.E. Lofland, A.K. Ganguli, Design of anisotropic Co_3O_4 nanostructures: control of particle size, assembly, and aspect ratio, Crystal Growth and Design 12 (2012) 4202−4210.

Figure and Table Captions

Fig. 1: XRD patterns of the as-prepared and calcined samples at 350 ^{o} and 500 ^{o}C.

Fig. 2: Thermal gravimetric analysis curves of the as-prepared sample.

Fig. 3: FT-IR spectra of the as-prepared and calcined samples at 350 ^{o} and 500 ^{o}C.

Fig. 4: XPS spectra of (a) Co_3O_4–ZnO mixed metal oxide nanoparticles, (b) Co 2p, (c) Zn 2p and (d) O 1s.

Fig. 5: Diffuse reflectance spectra of Co_3O_4–ZnO mixed metal oxide nanoparticles: (a) after calcination at 350 ^{o}C, (b) after calcination at 500 ^{o}C, and the plots (c) and (d) for $(\alpha h\upsilon)^2$ versus $h\upsilon$ drawn from the data (a) and (b).

Fig. 6: SEM images of samples (a) as-prepared, (b) calcined at 350 ^{o}C, (c) calcined at 500 ^{o}C, and (d) EDX analysis plot of Co_3O_4–ZnO mixed metal oxide nanoparticles.

Fig. 7: (a)-(b) TEM images, (c) corresponding SAED pattern of Co_3O_4–ZnO mixed metal oxide nanoparticles and (d) schematic model of the mixed metal oxide nanoparticles.

Fig. 8: Field-dependent magnetization (*M–H*) curves recorded at 10 K and 300 K for Co_3O_4–ZnO mixed metal oxide nanoparticles.

Fig. 9: Schematic of the exchange bias mechanisms.

Fig. 10: ZFC and FC curves for Co_3O_4–ZnO mixed metal oxide nanoparticles.

Table 1: BET surface area of the samples before and after calcination.

Table 2: EDXA data of the calcined samples at 350 ^{o} and 500 ^{o}C.

Table 1:

Sample	Surface area (m^2 g^{-1})
As-prepared	16.7
Co_3O_4–ZnO (calcined at 350 ^oC)	72.4
Co_3O_4–ZnO (calcined at 500 ^oC)	67.8

Table 2:

Sample	Element	At%	Wt%	Co/Zn
Co_3O_4–ZnO (calcined at 350 ^oC)	Co	35.56	56.43	2.98
	Zn	11.92	20.97	
	O	52.52	22.60	
Co_3O_4–ZnO (calcined at 500 ^oC)	Co	37.32	57.75	3.00
	Zn	12.44	21.36	
	O	49.76	20.89	

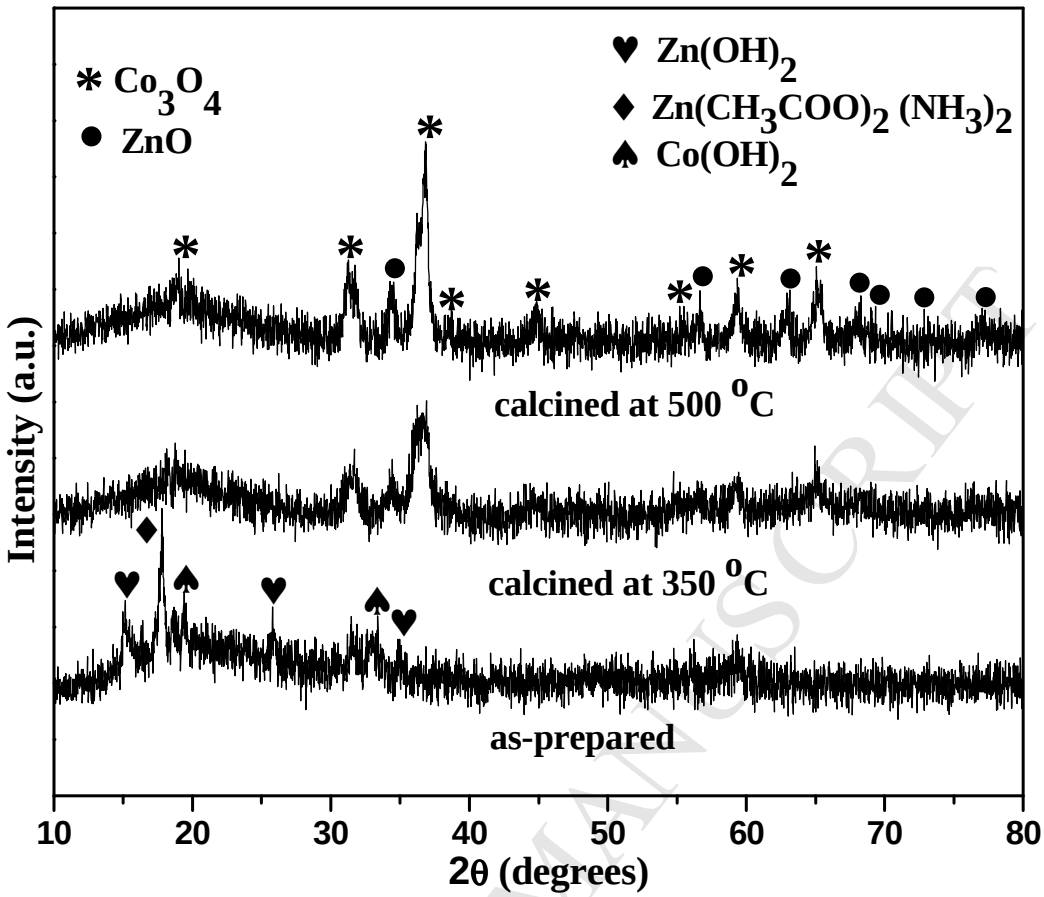

Fig. 1:

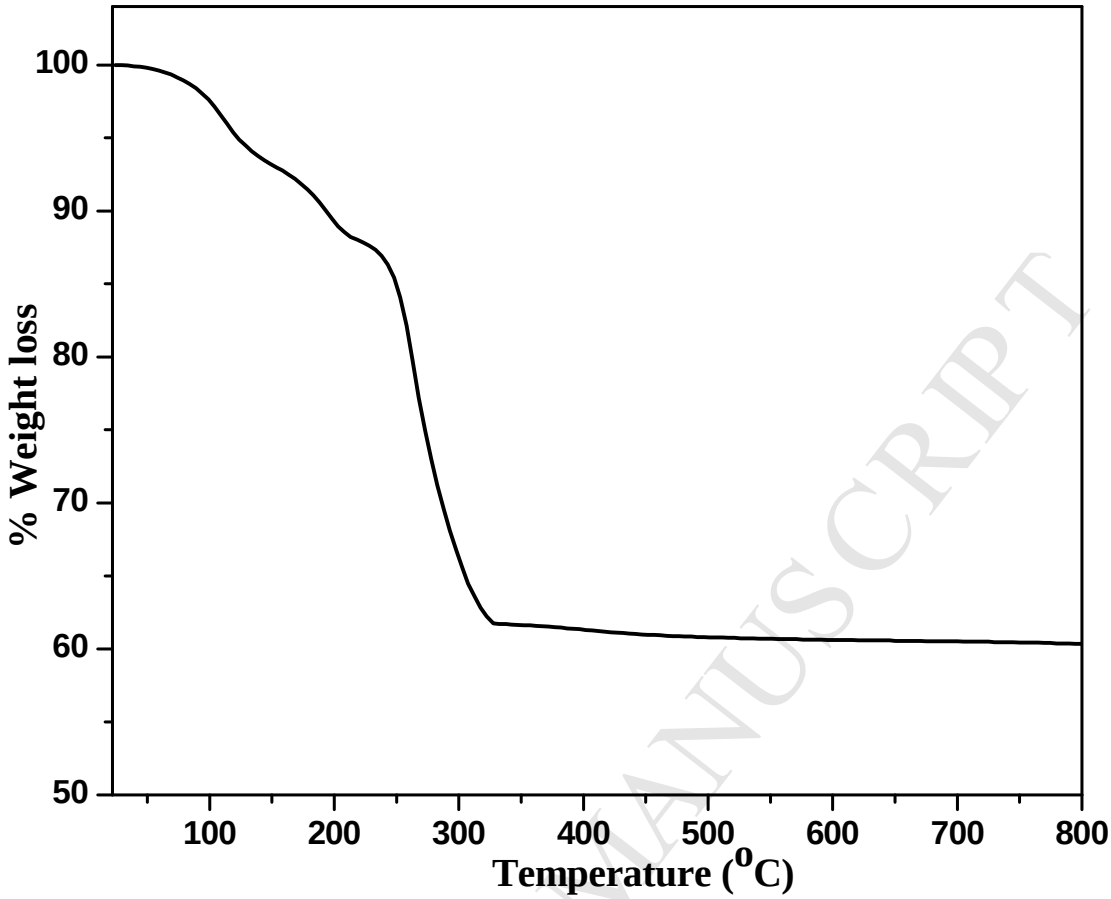

Fig. 2:

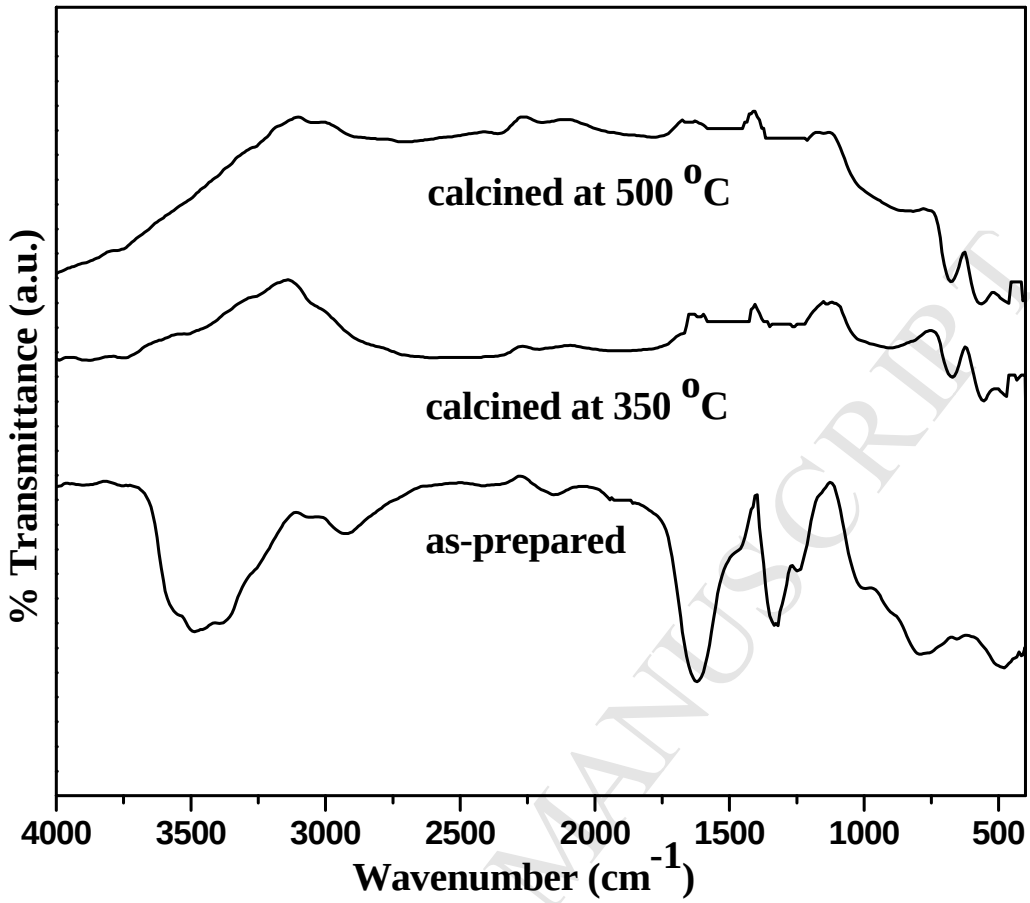

Fig. 3:

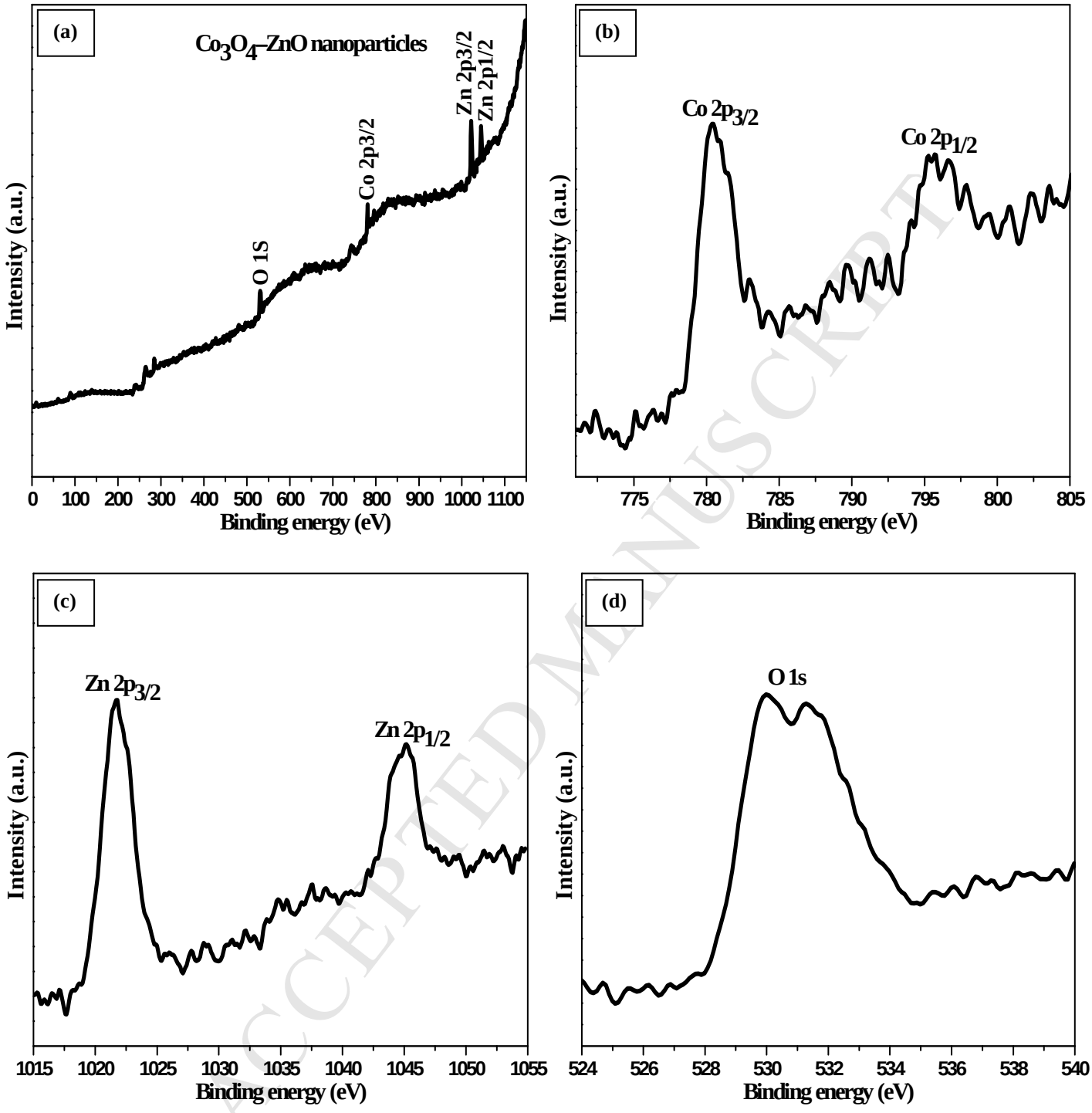
(a)
Co3O4–ZnO nanoparticles
O 1S
Co 2p3/2
Zn 2p3/2
Zn 2p1/2
Intensity (a.u.)
Binding energy (eV)
(b)
Co 2p3/2
Co 2p1/2
Intensity (a.u.)
Binding energy (eV)
(c)
Zn 2p3/2
Zn 2p1/2
Intensity (a.u.)
Binding energy (eV)
(d)
O 1s
Intensity (a.u.)
Binding energy (eV)

Fig. 4:

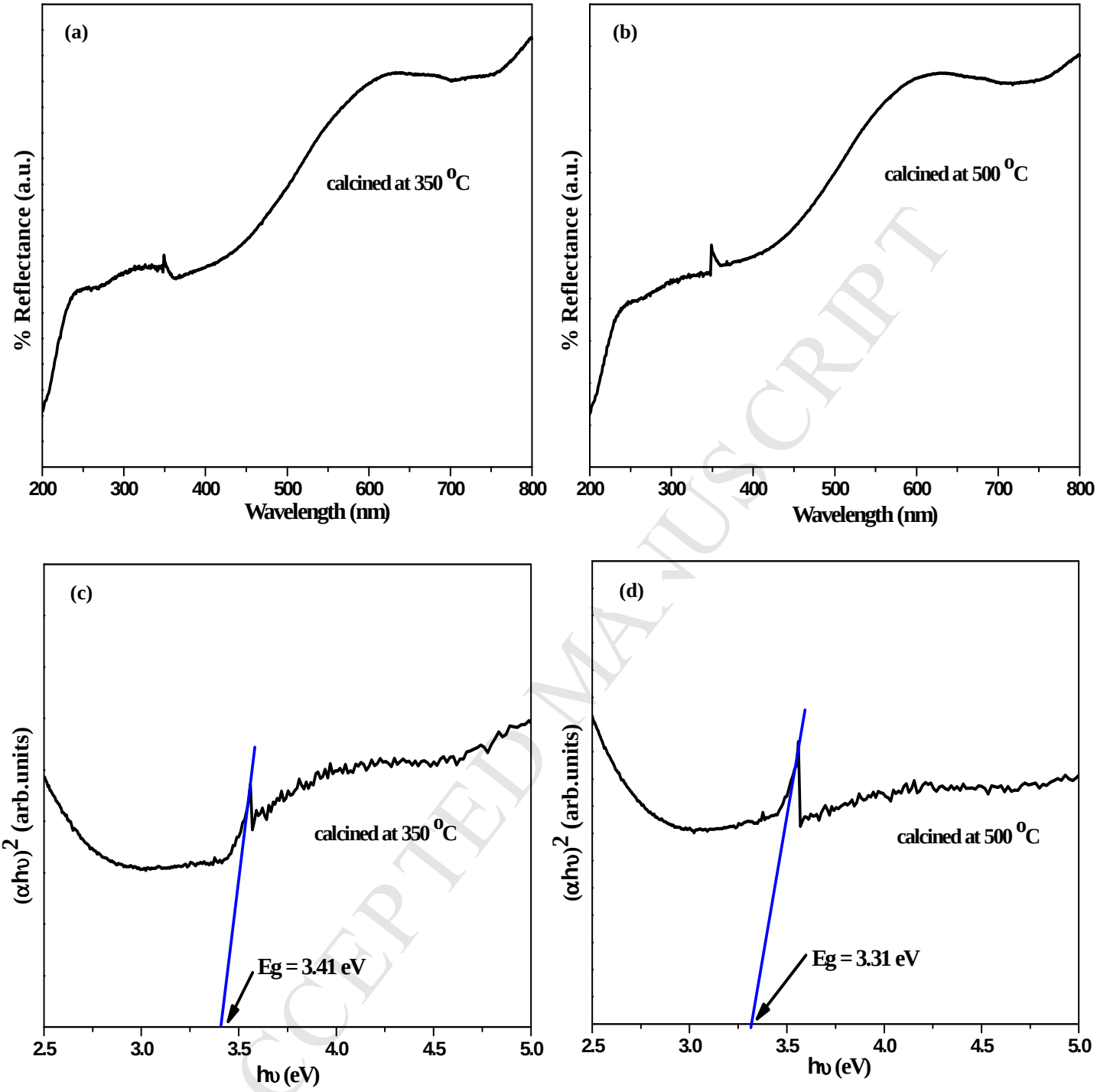

Fig. 5:

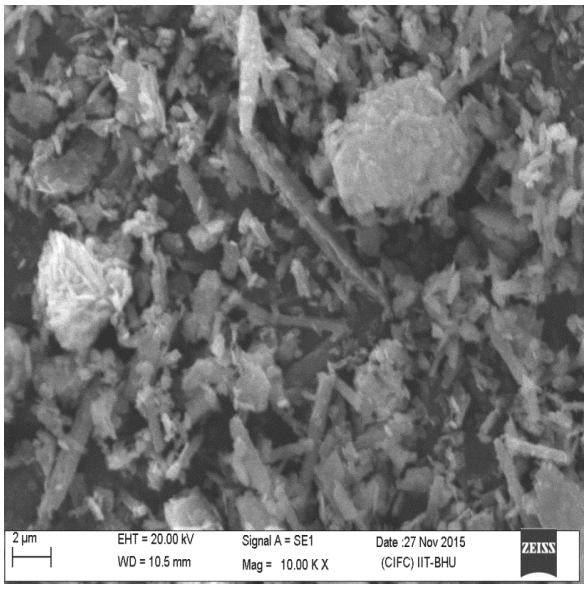
2 µm
EHT = 20.00 kV
WD = 10.5 mm
Signal A = SE1
Mag = 10.00 K X
Date :27 Nov 2015
(CIFC) IIT-BHU
ZEISS

(a)

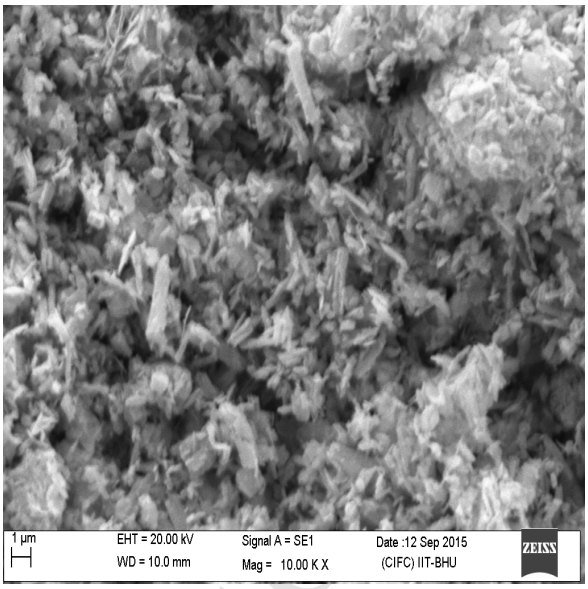
1 µm
EHT = 20.00 kV
WD = 10.0 mm
Signal A = SE1
Mag = 10.00 K X
Date :12 Sep 2015
(CIFC) IIT-BHU
ZEISS

(b)

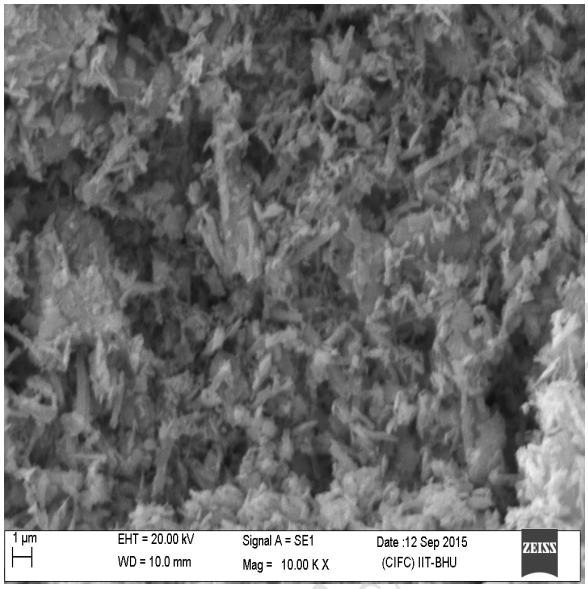
1 µm
EHT = 20.00 kV
WD = 10.0 mm
Signal A = SE1
Mag = 10.00 K X
Date :12 Sep 2015
(CIFC) IIT-BHU
ZEISS

(c)

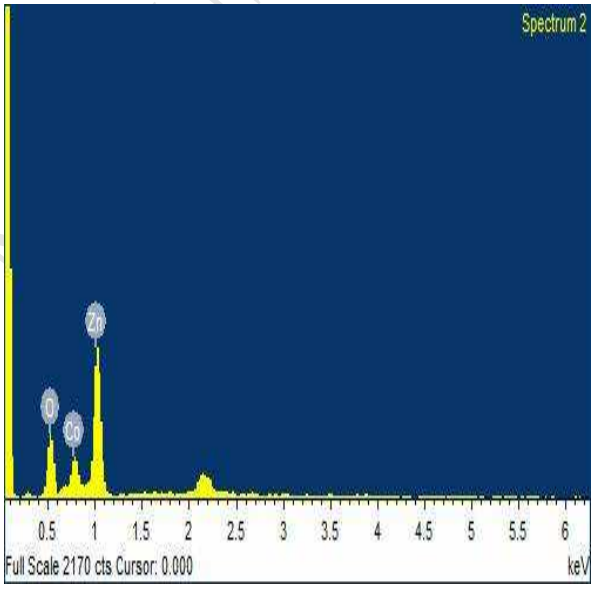
Spectrum 2
Zn
O
Co
0.5
1
1.5
2
2.5
3
3.5
4
4.5
5
5.5
6
Full Scale 2170 cts Cursor: 0.000
keV

(d)

Fig. 6:

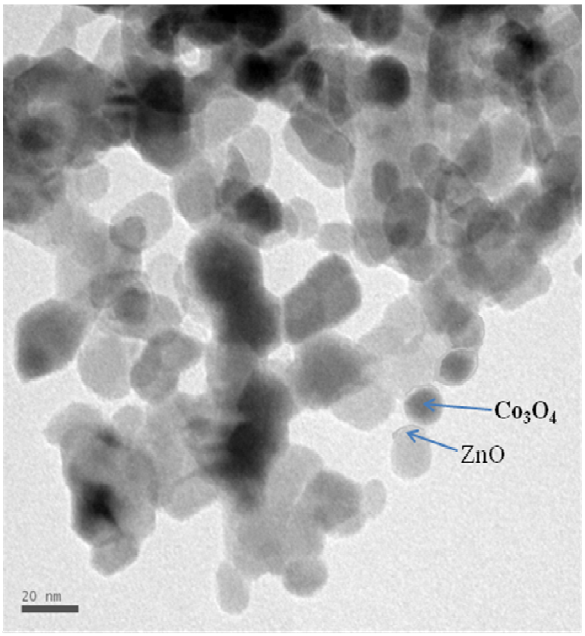

(a)

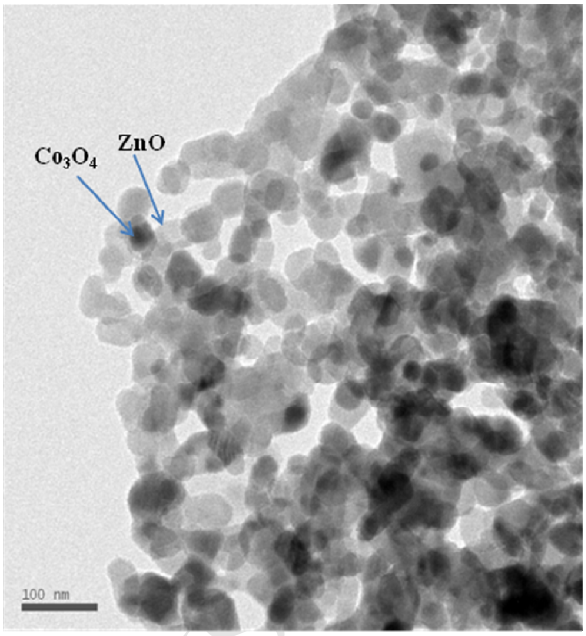

(b)

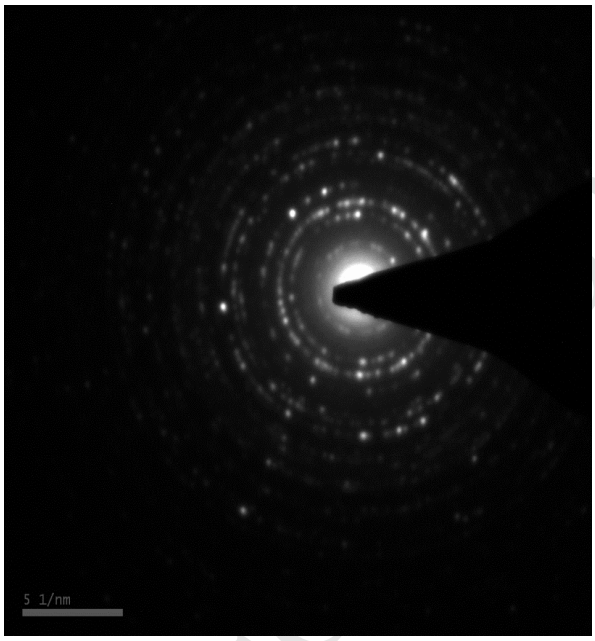

(c)

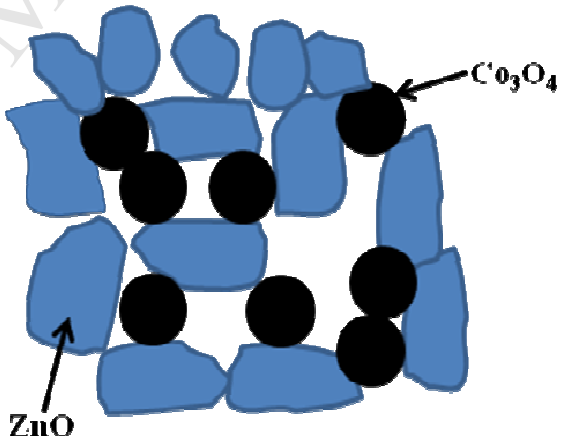

(d)

Fig. 7:

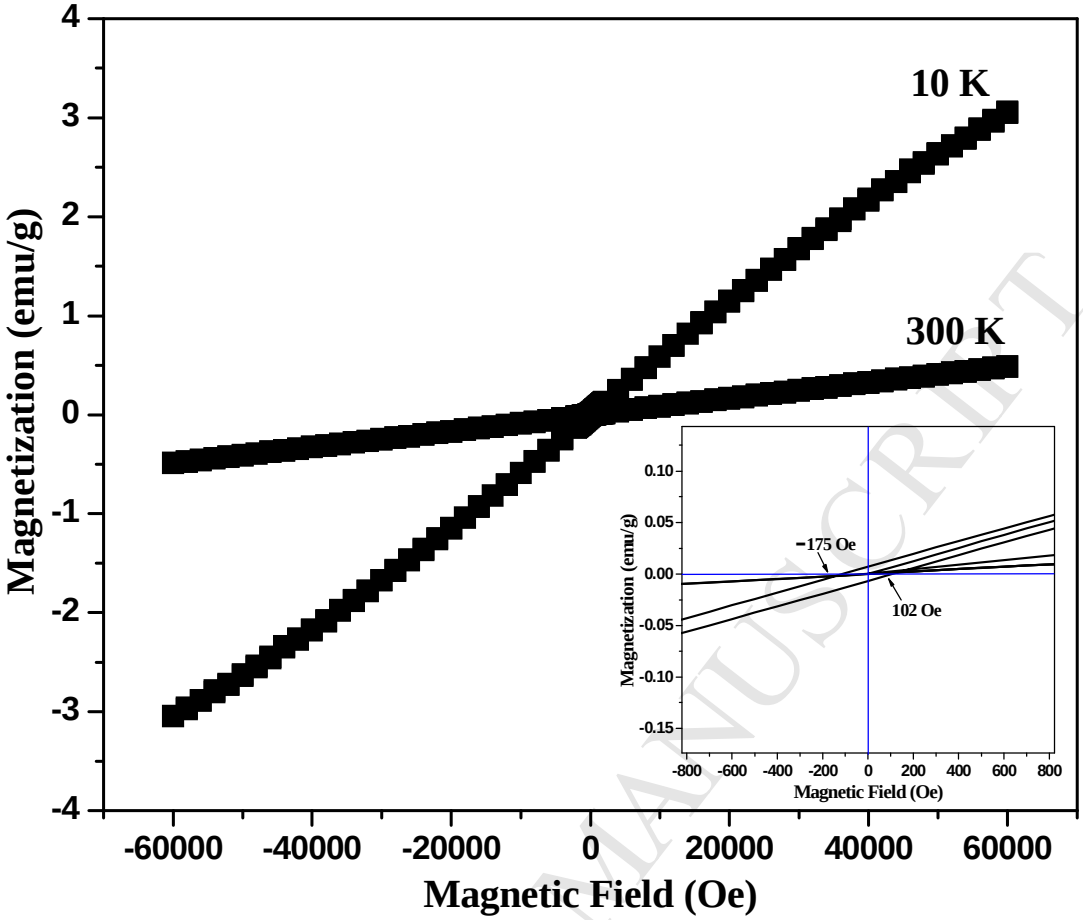
10 K
300 K
Magnetization (emu/g)
Magnetic Field (Oe)
4
3
2
1
0
-1
-2
-3
-4
-60000
-40000
-20000
0
20000
40000
60000
0.10
0.05
0.00
-0.05
-0.10
-0.15
-175 Oe
102 Oe
-800
-600
-400
-200
0
200
400
600
800

Fig. 8:

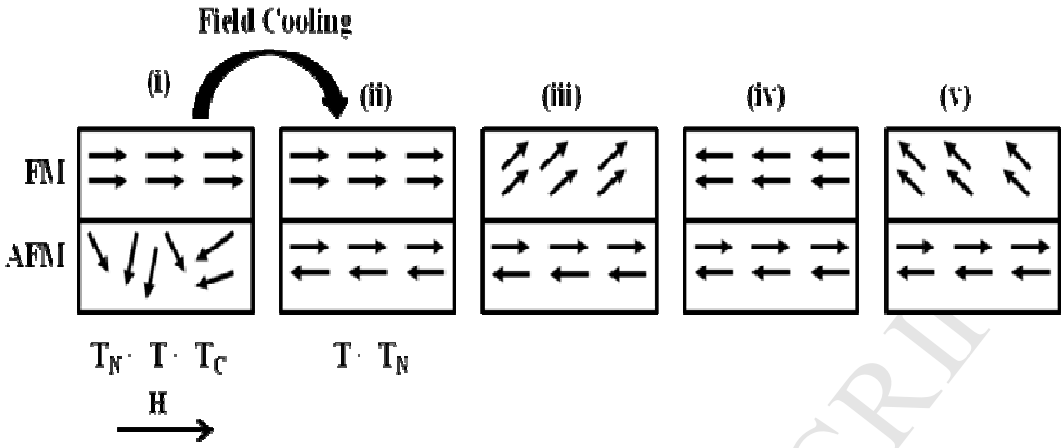

Fig. 9:

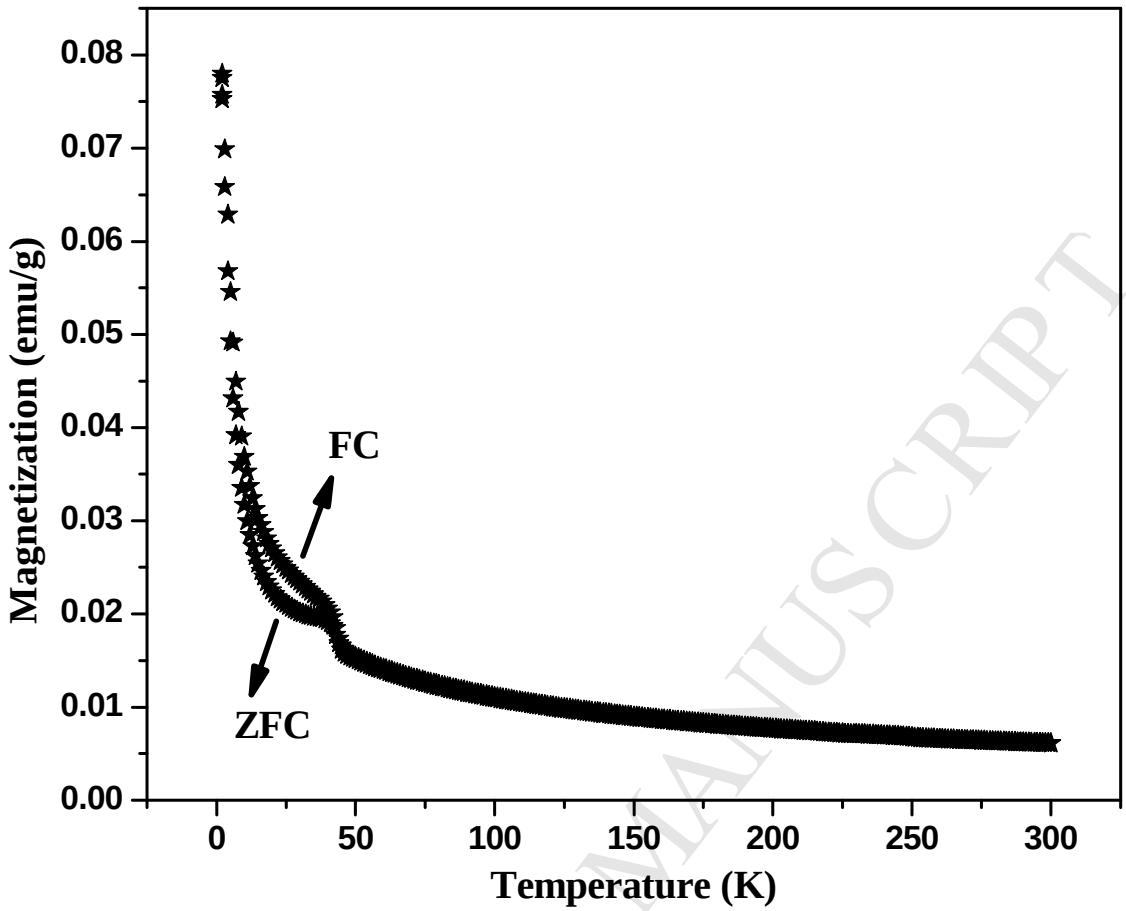

Fig. 10:

Highlights

- Co_3O_4–ZnO mixed metal oxide nanoparticles have been prepared by a simple homogeneous precipitation route.
- An easy and surfactant-free method is employed for its synthesis on a large scale in short time.
- Co_3O_4–ZnO mixed metal oxide nanoparticles exhibit weak ferromagnetic behavior at low temperature.